Energy and Built Environment xxx (xxxx) xxx

Contents lists available at ScienceDirect

Energy and Built Environment

journal homepage: http://www.keaipublishing.com/en/journals/energy-and-built-environment/

The thermal analysis of the heat dissipation system of the charging module integrated with ultra-thin heat pipes

Tingzhen Ming[a], Xiwang Liao[a], Tianhao Shi[a], Kui Yin[b], Zhiyi Wang[a], Mohammad Hossein Ahmadi[c], Yongjia Wu[a,*]

[a] School of Civil Engineering and Architecture, Wuhan University of Technology, Wuhan 430070, China
[b] China Constuction Third Bureau First Engineering Co. LTD. Wuhan 430040,China
[c] Faculty of Mechanical Engineering, Shahrood University of Technology, Shahrood, Iran

ARTICLE INFO

Keywords:
ICEPAK simulation
Charging pile
heat transfer
Ultra-thin heat pipe
Chip cooling

ABSTRACT

Electric vehicles (EV) played an important role fighting greenhouse gas emissions that contributed to global warming. The construction of the charging pile, which was called as the "gas station" of EV, developed rapidly. The charging speed of the charging piles was shorted rapidly, which was a challenge for the heat dissipation system of the charging pile. In order to reduce the operation temperature of the charging pile, this paper proposed a fin and ultra-thin heat pipes (UTHPs) hybrid heat dissipation system for the direct-current (DC) charging pile. The L-shaped ultra-thin flattened heat pipe with ultra-high thermal conductivity was adopted to reduce the spreading thermal resistance. ICEPAK software was used to simulate the temperature and flow profiles of the new design. And various factors that affected the heat dissipation performance of the system were explored. Simulation results showed that the system had excellent heat dissipation capacity and achieved good temperature uniformity. Rather than solely relied on the fans, this new design efficiently dissipated heat with a lower fan load and less energy consumption.

1. Introduction

With the advantages of cleanliness and efficiency, the electric vehicle (EV) showed great potential in reducing greenhouse gas emissions and environmental pollution [1]. As early as 2011, the European Union proposed a ban on the sale of traditional fuels vehicle. Then China, France, the United Kingdom, Norway, and some other countries also announced deadlines of stopping the production of conventional fuel vehicles. Simultaneously, funds and policies were also established to support the development of EVs [2], hoping to alleviate the global warming trend [3]. In recent years, the Chinese government had been committed to the popularization and application of EV [4]. The government had provided subsidies for the sale of EVs based on vehicle prices and greenhouse gas emission levels [1, 5]. China had become one of the most active countries in promoting the development of EVs [6].

EV DC charging piles mainly consisted of the power input modules, power modules, charging buses, fans, charging control units, electric energy metering units, and human-computer interaction units, etc. [7]. The progress of the charging pile technology, particularly the charging speed, was crucial to the development of EVs [8]. On the one hand, the facilities such as batteries and cables should be updated to meet the needs for fast charging. On the other hand, the heat dissipation system inside the charging pile should also be improved. However, because the heat flux density of the new generation of EV DC charging pile could reach 100 W/cm^2 [9], the increase in temperature significantly affected the reliability of the charging module [10]. It was reported that the reliability of electronics was halved for every 10°C increase in the operating temperature [11]. If the dissipation system was not well designed, the reliability of electronic devices and the service life could be reduced by two-thirds [12], and thermal runaway was a severe safety problem [4].

Currently, the heat dissipation design of the DC charging piles for EVs mainly adopted the forced air convection driven by the fans [13]. However, due to the miniaturization of the chip, the surface for the heat convection was limited [14]. Therefore, the fans with higher power were widely adopted for the charging pile cooling. However, the use of higher power not only increased the energy consumption and operating costs, but also generated strong noise during the operation. Many efforts in the field of electronic thermal management have focused on developing cooling solutions that cater to steady-state operation [10b]. Ryan et al. [15] believed that the heat generation of the cabinet integrated with multiple chips had reached the limit of the forced convection heat dissipation. There was an urgent need for the design of a

Abbreviations: EV, Electric vehicle; UTHP, Ultra-thin heat pipes.

* Corresponding author.
E-mail address: yjwu2019@whut.edu.cn (Y. Wu).

https://doi.org/10.1016/j.enbenv.2022.03.007
Received 27 December 2021; Received in revised form 4 March 2022; Accepted 30 March 2022
Available online xxx

Please cite this article as: T. Ming, X. Liao, T. Shi et al., The thermal analysis of the heat dissipation system of the charging module integrated with ultra-thin heat pipes, Energy and Built Environment, https://doi.org/10.1016/j.enbenv.2022.03.007

Nomenclature

$\bar{\bar{\tau}}$	Stress tensor (Pa)
c_p	Thermal capacity ($J \cdot K^{-1} \cdot kg^{-1}$)
P	Pressure (Pa)
Pr_t	Turbulent Prandtl number
κ	Von Kármán constant
I	Unit tensor
S_{ij}	Mean strain rate
t	Time (s)
T	Temperature (K)
L_p	Effective length of the heat pipe (m)
l	Mixing-length (m)
h	Sensible enthalpy (J)
S_h	Source term for the energy equation
$T_{uni}^{'}$	Uniformity index
S	Modulus of the mean rate-of-strain tensor
R_{th}	Effective thermal resistance of the heat pipe ($K \cdot W^{-1}$)
K_{eff}	Turbulent dissipation rate ($W \cdot m^{-1} \cdot K^{-1}$)
k	Molecular conductivity ($W \cdot K^{-1} \cdot m^{-2}$)
μ	Dynamic viscosity ($kg \cdot m^{-1} \cdot s^{-1}$)
ρ	Density ($kg \cdot m^{-3}$)

new and efficient heat dissipation system. Many researchers had done tremendous work to explore high-efficient and feasible electronics heat dissipation method. In order to improve the power density of electronic packaging, innovation and improvement in heat transfer were urgent [16]. The heat pipe, which had an axial high thermal conductivity [17], was considered to be one of the most efficient phase change heat exchangers. The heat pipe owned many good characteristics, such as good starting performance, compact and flexible geometry design [18], high heat transfer efficiency, excellent temperature uniformity and high reliability [19]. The traditional heat pipes had cylindrical shells, but in practical engineering, heat pipes were usually compressed into UTHPs through various technical means to meet the narrow space and structural requirements for electronic equipment [20]. Aoki et al.[21] proposed a use of a high-temperature redox sintered mesh as the wick for UTHPs with a thickness of less than 1.0 mm. They made and tested the heat transfer characteristics of a UTHP with a thickness of 0.7 mm and 1 mm, respectively, and verified that this structure had the high capillary force to provide the circulating power for the working fluid. Zhou et al. [22] developed a new UTHP with a helical braided mesh wick, which not only improved the heat dissipation power of the heat pipe, but also reduced the weight of the heat pipe by 64.51%. Such UTHP was used for the heat dissipation of smart phones. They [23] also proposed a new type of UTHP with a two-hole spiral woven mesh wick, which saved production costs and achieved the high thermal performance requirements of UTHPs. M. Ivanova et al. [24] proposed a flat radial structure silicon heat pipe, established a one-dimensional two-phase flow model, and tested the heat transfer performance of the samples. It was found that the heat transfer power of the modified UTHP was in the range of 50-70 W.

The emergence of ultra-thin flattened heat pipes technology was an important breakthrough in developing the heat dissipation system of electronic devices [25]. Its structure (shown in Fig. 1 [26]) consists of three parts in the length direction: evaporator, condenser, and adiabatic section, in which the adiabatic passage connects the evaporator and condenser [24, 27]. Generally, the thickness of the ultra-thin flattened heat pipe was less than 2.0 mm [28]. The UTHP was especially suitable for the heat dissipation of electronic equipment in narrow space. Thus it could be directly attached to the surface of the electronic components [29] to cool the heat source. However, few researches reported on the application of UTHPs to the heat dissipation of the DC EV charging piles.

Table 1
Dimensions and heating power of each device.

Component name	Size(mm)	Heating power(W)
Crate	206×470×83	0
PFC capacitor	Radius=20;height=50	20
Heating chips	5×140×60	100
Heat dissipation fins	10×140×1	0

In this paper, a numerical model was built to simulate the heat dissipation performance of the charging module with ultra-thin heat pipes integrated. The simulation model was validated by the experimental results of a product with the conventional thermal design. To further explore the factors that influencing the heat dissipation performance of the charging module, the temperature of the chip under different air volume rate and fin thicknesses were compared. This research could provide some useful guidelines for the thermal design of the charging modules.

2. Computational method

2.1. Geometric model

The geometric model was established based on the 20 kW charging module of the DC charging pile produced by a company and had been put into use, as shown in Fig. 2(a). The overall geometric size of the charging module was 206×470×83 mm^3. The shell thickness was 2 mm. The module was equipped with two fans with toal air volume of 134.292 CFM. As shown in Fig. 2 (b), its internal structure consisted a charging chip, a PFC capacitor, an isolation transformer, an input differential mode inductance, an input insurance, etc. According to the power curve of the product, the maximum efficiency of the charging module could reach 96%. The corresponding module load rate was in the range of 45%-55%. However, when the module was fully loaded, its efficiency reduced to 95%. The entire charging pile was equipped with 16 such charging piles, with a total heat load of 16 kW. It took 2~3 hours to complete a charge, which meant that the charging module need to be fully loaded for at least 2 hours, so the heat dissipation problem of the charging module was imminent. In this simulation, the thermal modeling of each device in the module was carried out under the full load working condition of the module, as shown in Fig. 3. The dimensions and heating power of each device were shown in Table 1.

2.2. Numerical model

2.2.1. Governing equations

This simulation was conducted by ANSYS ICEPAK 15.0. The ICEPAK 15.0 software uses the FLUENT 15.0 solver for calculation [30]. The temperature field distribution inside the module was calculated to study the heat dissipation problem of the electronics. The modeling results could directly and quantitatively guide the better thermal design. The fundamental governing equations, including the continuity, momentum, and energy conservation equations, were demonstrated below.

Continuity equation

$$\frac{\partial \rho}{\partial t} + \nabla \cdot \vec{u} = 0 \tag{1}$$

Momentum equation

$$\frac{\partial}{\partial t}(\rho \vec{v}) = -\nabla p + \nabla \cdot (\bar{\bar{\tau}}) + \rho \vec{g} + \vec{F} \tag{2}$$

where stress tensor $\bar{\bar{\tau}} = \mu[(\nabla \vec{v} + \nabla \vec{v}^T) - \frac{2}{3}\nabla \cdot \vec{v} I]$, $\boldsymbol{I}$ was the unit tensor, $(\nabla \vec{v} + \nabla \vec{v}^T)$ represented the effect of volume dilation, μ represented the molecular viscosity, $\vec{F}$ was the other source terms that may arise from resistances, sources, and so on. The specific parameters were set by the user independently.

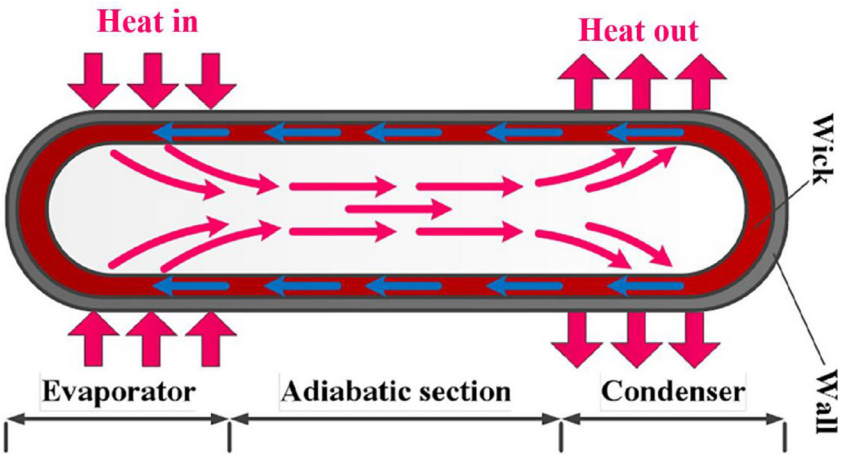

Fig. 1. The structure of UTHPs.

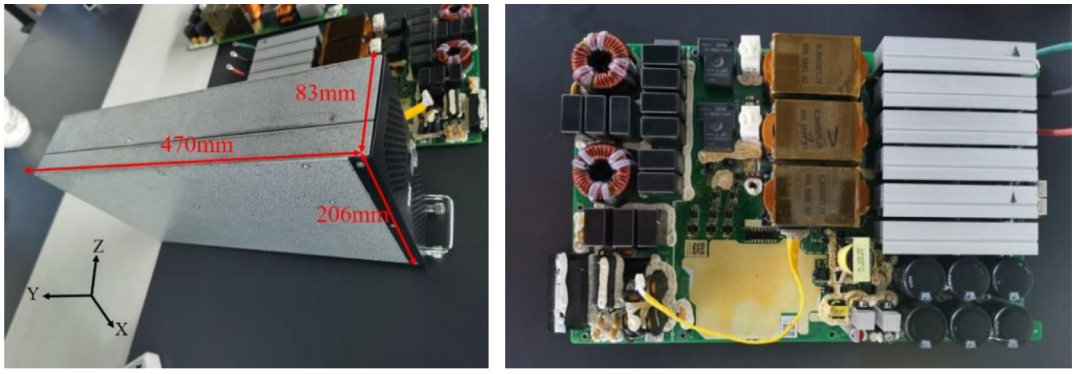

Fig 2. (a) The prototype of charging module; (b) the internal structure.

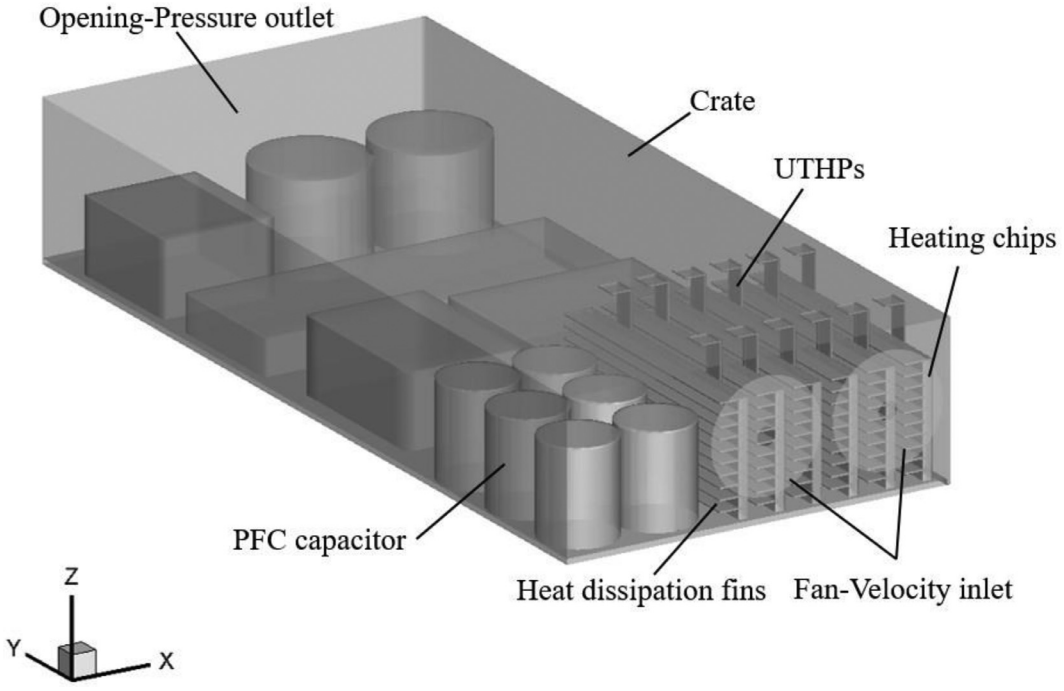

Fig. 3. The computational model.

Energy equation (fluid region)

$$\frac{\partial}{\partial t}(\rho h) = \nabla\left[\left(k + k_t\right)\nabla \mathrm{T}\right] + S_h \tag{3}$$

Energy equation (solid region)

$$\frac{\partial}{\partial t}(\rho h) = \nabla(k\nabla \mathrm{T}) \tag{4}$$

where h was the sensible enthalpy, $h = \int_{T_{ref}}^{T} c_p dT$, and T_{ref}=298.15K; k was the molecular conductivity; k_t represented the thermal conductivity due to turbulent transport, $k_t = c_p \mu_t / Pr_t$; S_h represented any volumetric heat sources.

2.2.2. Turbulence model

In this simulation, the flow volume at the inlet was set as 134.3 CFM with a Reynolds number of 87,317.6. The air was considered as an incompressible fluid. The zero-equation model [31] based on the mixing-length theory was selected for the turbulence modeling. The zero-equation model was selected because it was thought more robust and accurate to model the cases when the transition from the boundary layer to the mainstream layer was accidental [32]. The turbulent viscosity was calculated by the following relation

$$\mu_t = \rho \ell^2 S \tag{5}$$

where the mixing-length $l = min(xd, 0.09d_{max})$, d was the distance from the wall, and x = 0.419 represented the von Kármán constant, $S \equiv \sqrt{2S_{ij}S_{ij}}$ was the modulus of the mean rate-of-strain tensor, and $S_{ij} = \frac{1}{2}(\frac{\partial u_j}{\partial x_i} + \frac{\partial u_i}{\partial x_j})$ represented the mean strain rate.

2.3. The simplification of the heat pipe

The L-shaped UTHP was made from an 8 mm diameter round heat pipe with a length of 80 mm, which was flattened to a thickness of 1 mm, a width of 12.3 mm. Because the two-phase flow heat transfer inside the heat pipe [33] was complex, the heat pipe was simplified to a solid block with the same geometry and effective anisotropic thermal conductivities. The thermal conductivity in the thickness direction was set as 202.4 W/(m•K) [34], which was the thermal conductivity of the heat pipe body material made by 6061 aluminum alloy. The thermal conductivity in the heat transfer direction was K_{eff}, which was given by Eq. (6) [35].

$$K_{eff} = \frac{L_p}{AR_{th}} \tag{6}$$

where, L_p was the effective length of the heat pipe, A was the cross-sectional area of the heat pipe. In the study, these values were taken from the actual size of the heat pipe. R_{th} was the heat transfer resistance of the heat pipe, which is measured as 0.238 K/W. The K_{eff} of the heat pipe could be calculated by Eq. (6), which was 28,000 W/(m•K) [36].

2.4. Boundary conditions

The ambient temperature was set to 35 °C to make sure the device could work in most region around the world. Other components, such as chips and capacitors, were set as blocks with volume heat source. The fans were given an air volume of 134.3 CFM and set to the velocity-inlet. The opening was set as a pressure outlet with a relative pressure of 0 Pa. The module crate was set as an adiabatic wall with a given heat flow of 0 W.

2.5. Validation

The temperature profiles of the numerical model with grid numbers of 1,360,428, 2,239,482, and 3,370,419 were compared to check the grid independence. The chips from right to left were numbered as chips #1-#6, respectively. The temperature profile on the bisecting line in the height direction of chip #1 was taken as the basis for grid independence verification. As shown in Fig. 4, it was found that the differences were less than 3%, and it was considered that the modeling result was grid independent.

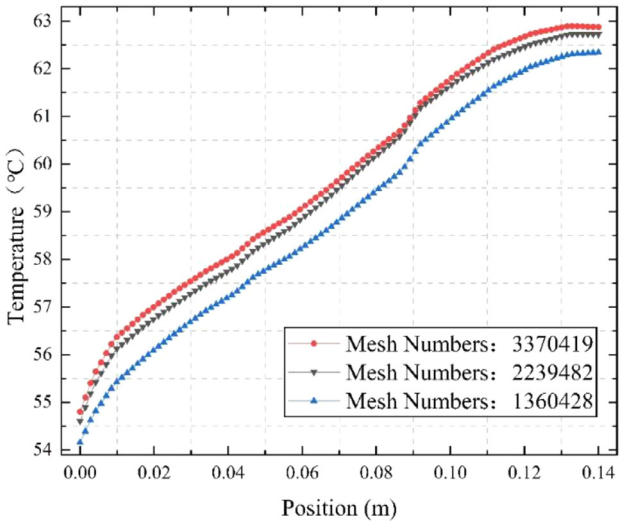

Fig. 4. Mesh independence verification.

Fig 5

To validate the accuracy of the numerical simulation, the DC charging pile were tested experimentally. The temperature values during the charging process were recorded. The temperature was recorded until the DC charging pile worked for 3.0 hours when it reached the steady state. The temperature values under the full load were used to validate the simulation result. The experimental and modeling results for the temperatures of five surfaces in the charging module was compared (Fig. 6). The average temperatures of the two PFC capacitors were also compared, as shown in Table 2. The relative errors of each item were calculated, which were all less than 10%.

3. Results and discussion

3.1. Optimal design of the heat dissipation system

3.1.1. Heat transfer performance enhanced by adding heat pipes

The evaporation section was close to the surface of the chip. The working fluid in the wick of the evaporation section absorbed part of the heat, and evaporated into steam and then reached the condensation section through the adiabatic passage. The steam released heat in the condensing section and condenses into liquid, and this part of the energy was transferred to the shell of the charging module through the condensing area. The working fluid that became liquid passes through the wick to return to the evaporation section under the combined action of capillary pressure and gravity to continue the above process. In this cycle, heat was transferred from the evaporating end of the tube to the condensing end.

Fig. 7. (a) showed the temperature distribution of the chip surface under the condition without the heat pipe. The lowest temperature was 45.89°C, the peak temperature was 63.01°C, and the mean temperature of the chip was 57.15°C. When two L-shaped UTHPs were attached to the surface of each chip, the minimum temperature of the chip surface was 35.79°C, the highest temperature was 48.21°C, and the average temperature was 42.82°C. The temperature distributions on the surface of the chip for the two cases were presented in Fig. 7.(b).

To study the heat dissipation effect of the heat pipe more intuitively, the temperature profile on the bisecting line in the direction of the chip height was selected as a reference, as shown in Fig. 8. It was found that the temperature of the chip was significantly reduced, the peak tem-

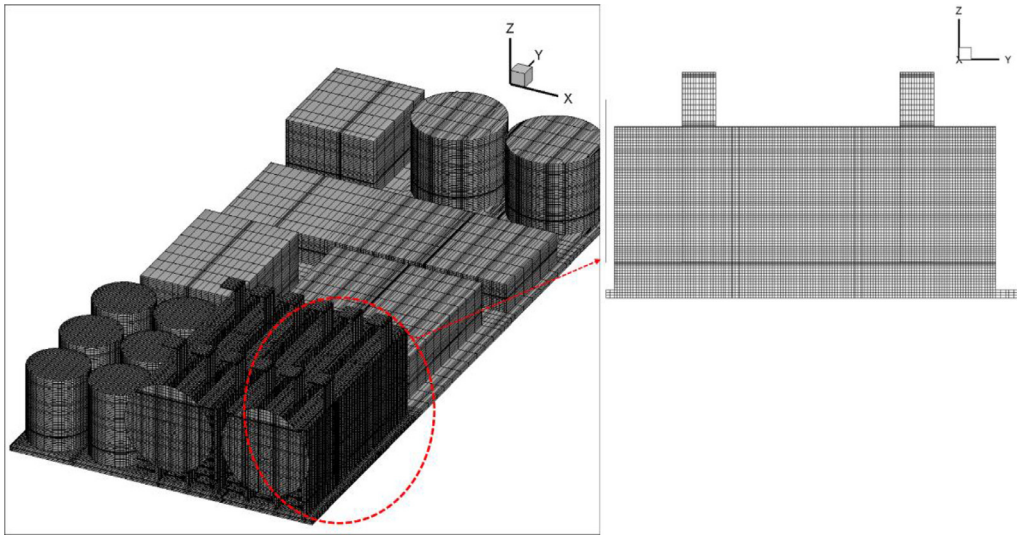

Fig. 5. Grid system of the model.

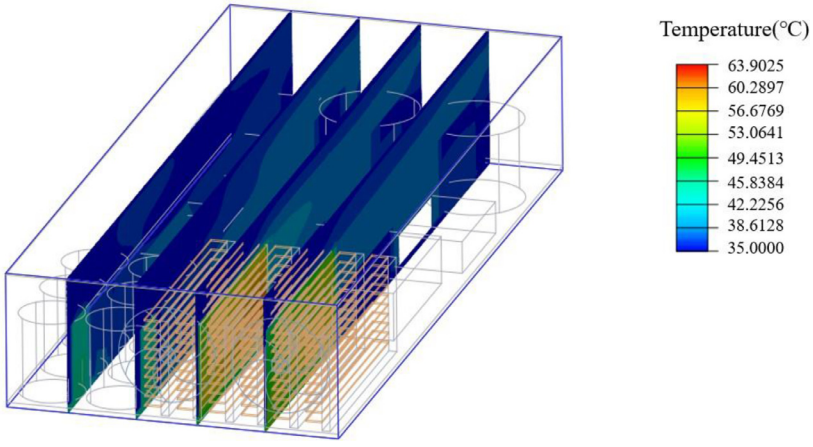

Fig. 6. Internal ambient temperature verification.

Table 2
Error analysis of comparison between simulation and experiment.

	Number of the measuring point	Experiment (°C)	Simulation result(°C)		Deviation
		Steady	Max	Mean	
PFC capacitor	116	49.745	45.969	45.347	8.771%
			46.169	45.417	
Ambient temperature	316	42.302	45.953	37.400	6.624%
			46.2023	37.800	
			61.892	41.900	
			55.7352	40.900	

perature was reduced by 15.35°C compared with the case without heat pipe, the temperature of the part close to the heat pipe was significantly reduced, and the local temperature difference reached 26.19°C.

3.1.2. Heat transfer performance variation with the fan air volume rate

In this section, the effect of the influence of the fan air volume on the heat dissipation performance of the charging module chip was studied.

The simulations were conducted for eight cases with different fan air volumes, including 74 CFM, 94 CFM, 114 CFM, 134 CFM, 154 CFM, 174 CFM, and 194 CFM, respectively. It could be seen in Fig. 9 that when the fan's air volume increased, the temperature of the chip surface gradually declined. The peak temperature and mean temperature of the chip under different fan volume rates were shown in Fig. 9. However, the temperature of the chip was not sensitive to the air volume rate. With the flow rate increased from 74 to 194 CFM, the temperature of the chip only decreased by about 1°C. This showed that the traditional heat dissipation method was low in efficiency and cannot rapidly and effectively cool down the internal components of the charging module.

In order to describe the heat dissipation situation more clearly. The temperature of the fin surface with the fan air volume rate was shown in Fig. 10. The temperature of the fin surface was lower than that of the chip surface, but their trends were the same. In the part close to the heat

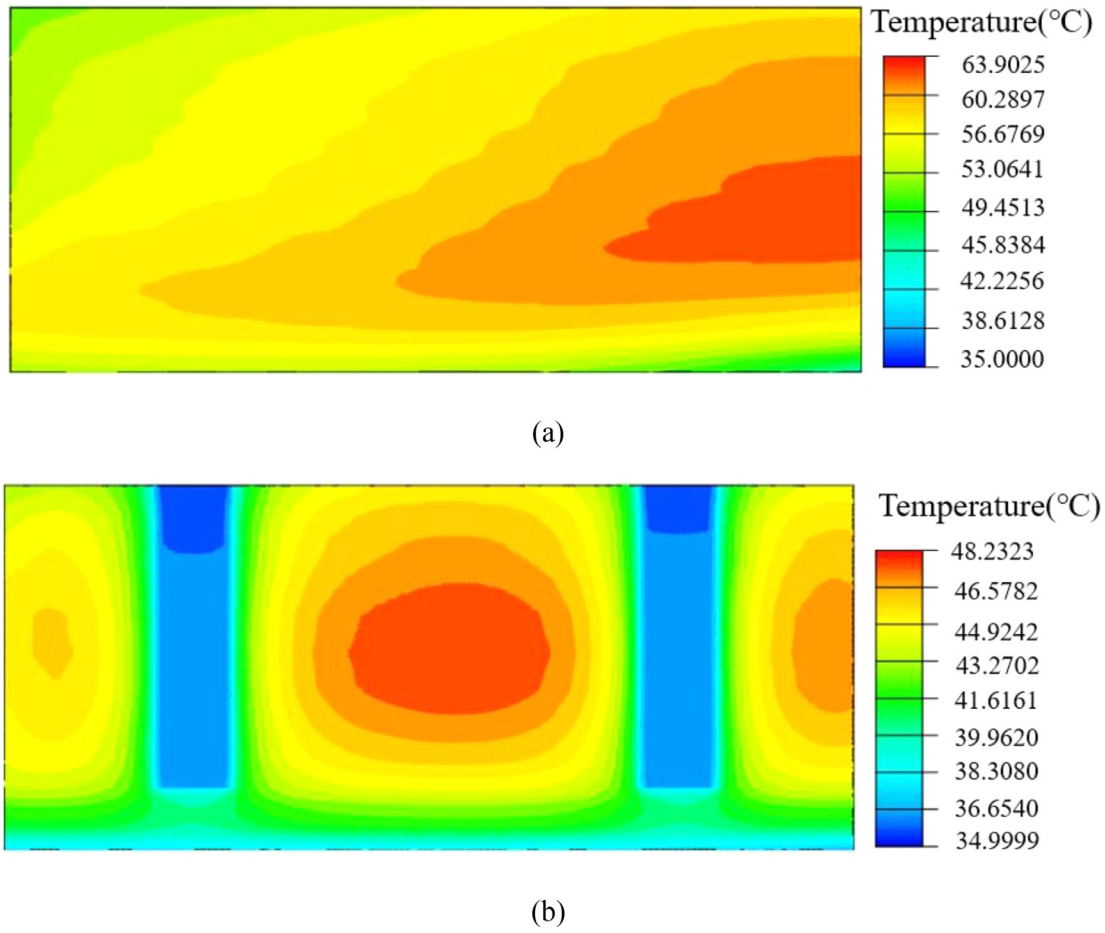

Fig. 7. (a)The temperature profiles on the surfaces of the chip without heat pipes; (b) The temperature profiles on the surfaces of the chip with heat pipes.

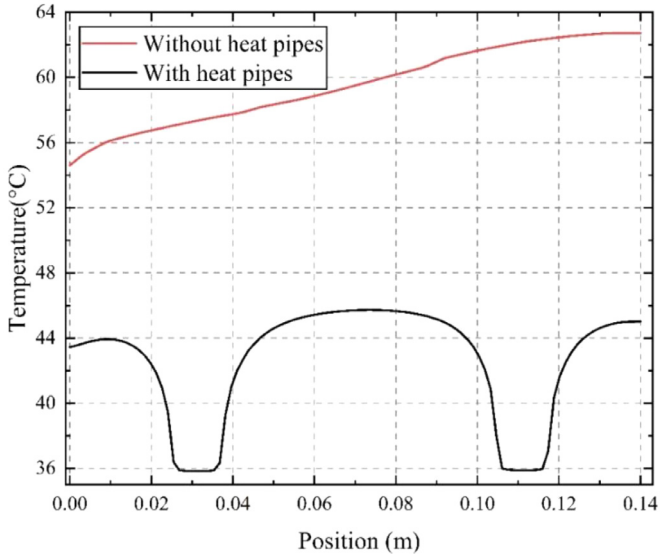

Fig. 8. The temperature profiles on the bisecting line of the chip surface.

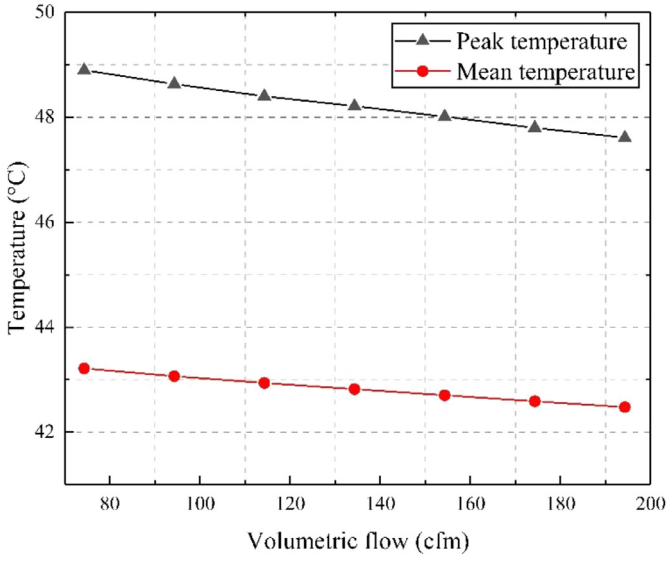

Fig. 9. Influence of flow rate.

pipe, the temperature of the fin surface was lower, which was consistent with the temperature curve shown in Fig. 8. With the increase of the fan air volume rate, the temperature of the fin surface decreased graduatlly. The decreasing trend was synchronized with the temperature of the chip surface.

3.1.2. Heat transfer performance variation with the fin thickness

The main function of the fins was to increase the heat exchange area and improve the heat dissipation efficiency of electronic devices [37]. The simulation was did for different fin thicknesses, including 1.0 mm, 1.5 mm, 2.0 mm, 2.5 mm, 3.0 mm, respectively. The surface tempera-

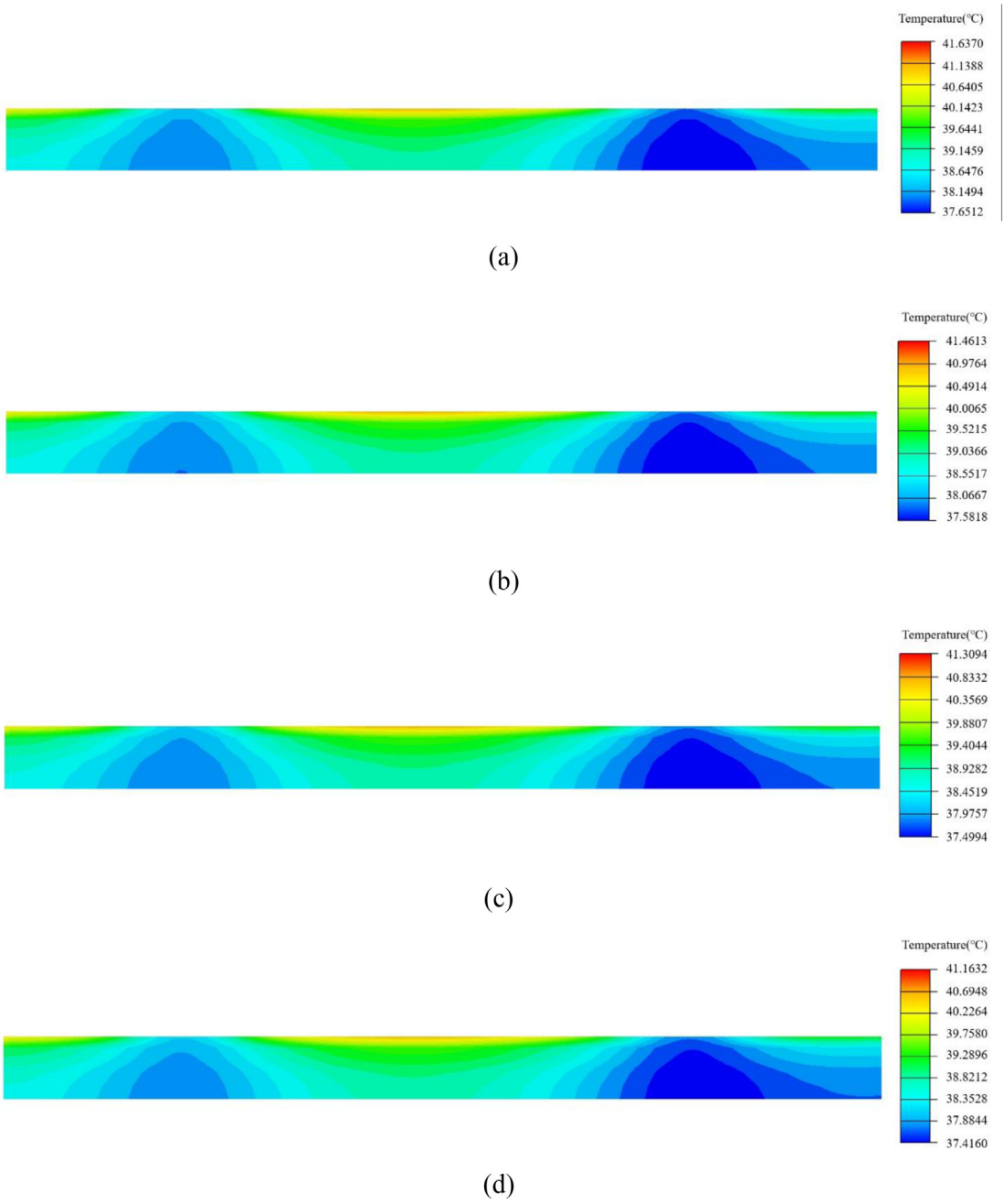

Fig. 10. The temperature contours of the fin surface with the fan air volume rate of (a)114CFM; (b)134CFM; (c)154CFM; (d)174CFM.

ture of chip #1 was shown in Fig. 11. The peak temperatures of each cases were draw in Fig. 12 for comparison. It could be found that the temperature of the chip decreased with the larger fin thickness. The fin thickness was increased from 1 mm to 3 mm. The peak temperature of the chip was reduced from 48.21˚C to 40.47˚C. Increase the fin thickness was more effective to reduce the chip temperature than increasing the air volume, as described in the previous section. However, as the fin thickness continued to increase, the heat dissipation effect would decrease, as shown in the Fig. 13. When the fin thickness reached 3.5mm, the best heat dissipation effect was achieved. As the fin thickness continued to increase, the surface temperature of the chip increased. This was because the increase of fin thickness lead to the narrowing of air flow channel between fins. Then the thermal boundary layers were disturbed, and the increase of fin thickness would hinder heat transfer [37].

3.2. Temperature uniformity of the chip

The purpose of thermal management was to ensure the high-performance and stable operation of electronic devices. The uniformity of the chip temperature had the significant impact on the service life. The uniformity index T_{uni} was introduced to quantify the temperature uniformity of the chips. The temperature uniformity index was defined by Eq. (7):

$$T_{uni} = \frac{T_{peak} - T_{min}}{T_{mean}} \tag{7}$$

where T_{peak} represented the peak temperature of the chip surface, T_{min} represented the lowest temperature of the chip surface, and T_{mean} represented the average temperature of the chip surface. According to the definition of uniformity index, the smaller the value, the better the tem-

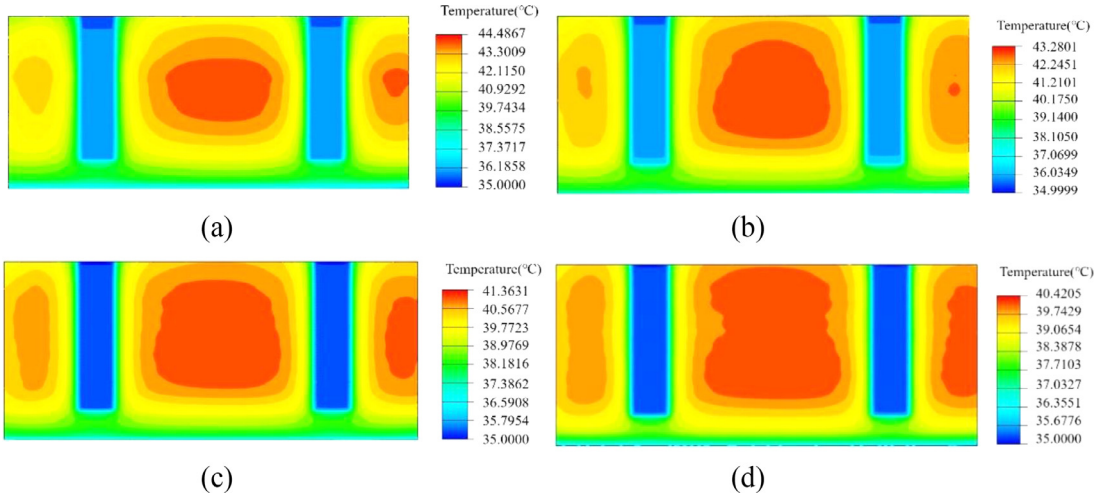

Fig. 11. The temperature of the chip surface with the fin thickness of (a)1.5mm; (b)2.0mm; (c)2.5mm; (d)3.0mm.

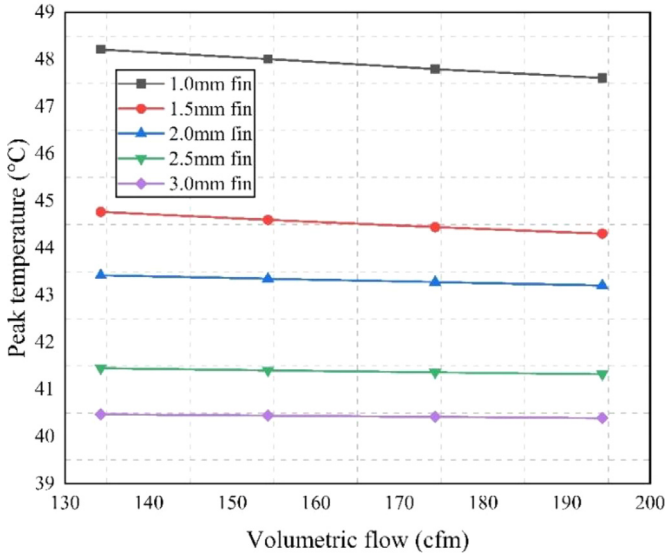

Fig. 12. The peak temperature of the chip under different flow rate and fin thickness.

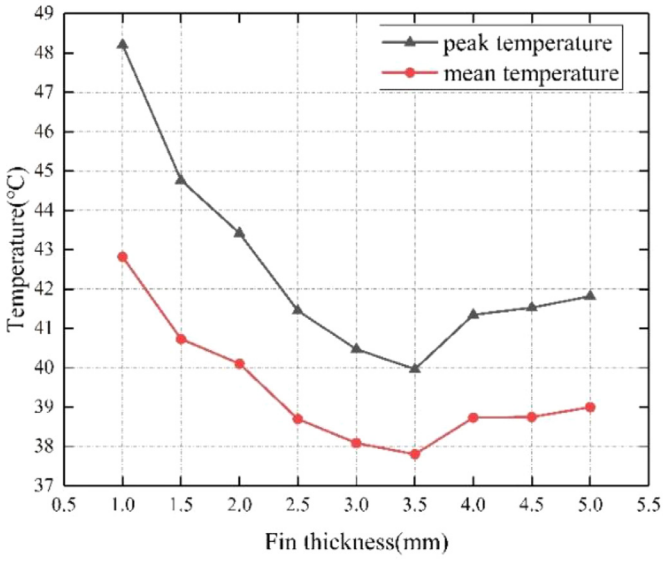

Fig. 13. The temperature of the chip under different fin thickness.

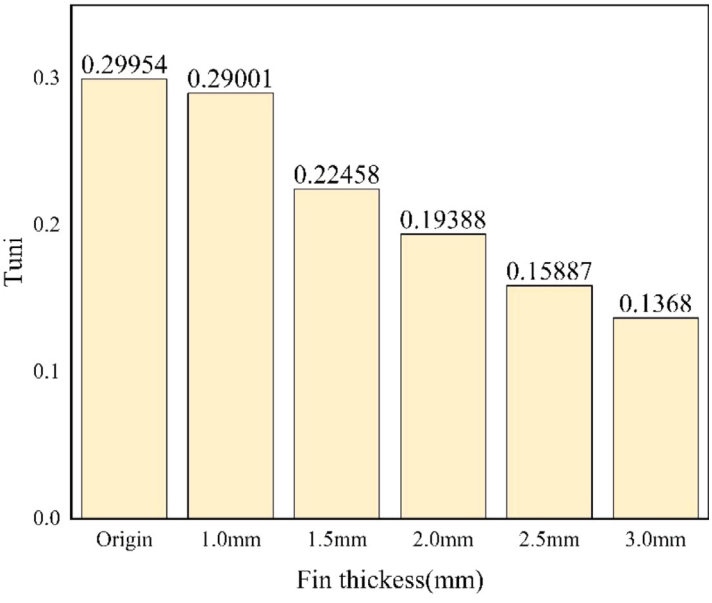

Fig. 14. Comparison of uniformity index when the flow rate was 134 cfm.

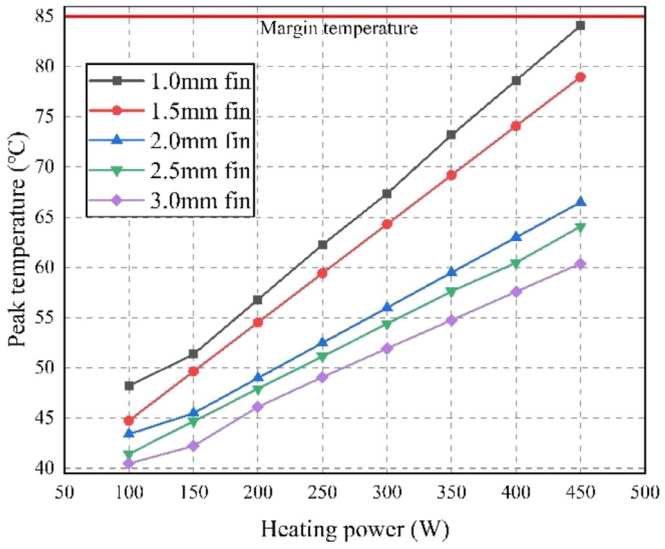

Fig. 15. The peak temperature of the chip varied with heating power and fin thickness.

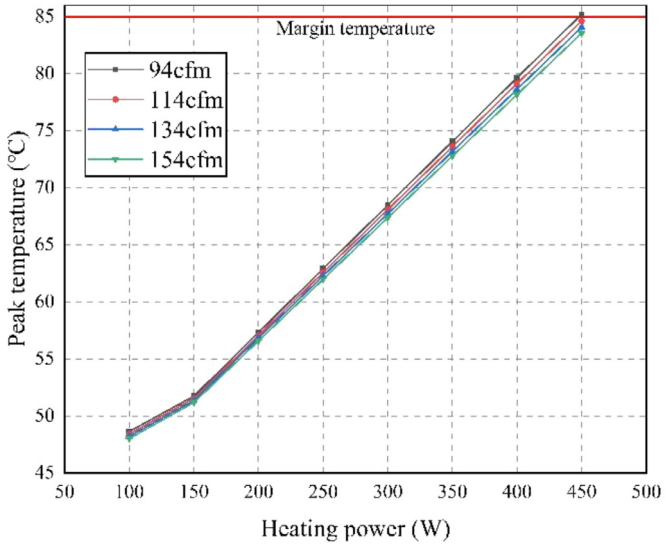

Fig. 16. The peak temperature of the chip varied with heating power and flow rate.

perature uniformity of the device [38]. The uniformity index of each case was summarized in Fig. 14. Since the fan air volume had a small effect on the heat dissipation, only the modeling results for the case with a flow rate of 134 CFM were presented. It was found that the hybrid heat dissipation system proposed in this paper significantly improved the temperature uniformity of the chip. Compared with the original heat dissipation method, the temperature uniformity index was reduced by about 54.3%, which could effectively increase the service life of the chip.

3.3. Overall heat dissipation capacity of the novel design

The peak temperature of the chip were studied with the heating power increased from 100 W to 450 W. According to the "Off-board bi-directional charger for electric vehicles general technical requirements" (Q/GDW 397-2009) formulated by Chinese government, the peak temperature of the chip should be lower than 85°C for safe and stable operation.

Fig. 14 and Fig. 15 showed the peak temperature of the chip with different fin thickness and flow rate. According to the analysis in Section 3.1.2, when the air volume reached 174 CFM, the temperature drops of the chip became unsensitive. As expected, the peak temperature of the chip increased with the heating power. The peak temperature of the chip increased about 10°C with the heating power increased by 100 W. When the heating power reached 450 W, the peak temperature of the chip was close to the margin temperature. When the heating power of a single chip was 450 W, the charging power of the entire module reached 54 kW, which was much higher than the rated charging power of the original product. With the increase in charging power, the charging speed of the module could be enhanced. The new heat dissipation design can better serve the fast charging of the charging piles Fig 16.

4. Conclusions

The influence of the fin design and flow rate on the heat dissipation capacity of the heat pipe-fin hybrid heat dissipation system were studied in this paper. The mathematical model was validated by the experiments before it was applied for the numerical simulation in this paper. The heat dissipation performance was evaluated by the peak temperature and temperature uniformity on the chip surface. According to the simulation results, the following conclusions can be drawn:

(1) UTHPs could significant enhance the heat dissipation capacity of the charging module. The peak temperature of the chip was reduced by about 17.71°C with the introduction of the UTHPs.
(2) The flow rate of the fan exhibited a weak influence on the heat dissipation performance of the charging module. With the flow rate increased by 20 CFM, the chip temperature reduction was less than 0.5 °C. When the fin thickness was less than 3.5 mm, the chip surface temperature decreased by 1-2°C with the fin thickness increased by every 0.5 mm. We could conclude that the heat dissipation effect of the UTHPs was the best, followed by the thickness of the fins, and finally the flow rate.
(3) It was found that the hybrid heat dissipation system could significantly improve the temperature uniformity of the internal chip of the charging module. Under the optimal working conditions, the chip uniformity index was reduced by 0.163, and its temperature uniformity performance was increased by 54.33%. The new thermal design could effectively reduce the thermal fatigue caused by non-uniform temperature distribution.
(4) The charging power of the original charging module increased from 20 kW to 54 kW using the hybrid heat dissipation system. The technical upgrade of the various accessories of the charging pile would ultimately increase the charging speed of EVs, making charging more efficient and convenient.

The hybrid heat dissipation system could effectively improve the heat dissipation efficiency of the charging pile. At the same time, it had advantages in improving temperature uniformity, fan noise reduction, and increasing charging speed. Based on the above, the hybrid heat dissipation system provided a certain reference for the heat dissipation system design of the charging piles.

Declaration of Competing Interest

The authors declare that they have no known competing financial interests or personal relationships that could have appeared to influence the work reported in this paper.

CRediT authorship contribution statement

Tingzhen Ming: Supervision, Conceptualization, Methodology, Software, Resources. **Xiwang Liao:** Investigation, Software, Writing – original draft. **Tianhao Shi:** Writing – review & editing, Visualization. **Kui Yin:** Writing – review & editing, Investigation. **Zhiyi Wang:** Software, Writing – review & editing, Investigation. **Mohammad Hossein Ahmadi:** Writing – review & editing, Visualization. **Yongjia Wu:** Supervision, Visualization, Validation.

Acknowledgements

This research was supported by the National Key Research and Development Plan (Key Special Project of Inter-governmental National Scientific and Technological Innovation Cooperation, Grant No. 2019YFE0197500), Key Research and Development Projects of Hubei Province (Grant No. 2020BAB129), the Scientific Research Foundation of Wuhan University of Technology (Grant Nos. 40120237 and 40120551), and the Fundamental Research Funds for the Central Universities (Grant No. WUT: 2021IVA037).

References

[1] J. Lin, X. Liu, S. Li, C. Zhang, S. Yang, A review on recent progress, challenges and perspective of battery thermal management system, Int. J. Heat Mass Transfer 167 (2021) 120834.
[2] (a) J. Chen, E. Jiaqiang, S. Kang, X. Zhao, H. Zhu, Y. Deng, Q. Peng, Z. Zhang, Modeling and characterization of the mass transfer and thermal mechanics of the power lithium manganate battery under charging process, Energy 187 (2019) 115924; (b) F. Nazari, E. Rahimi, A.K. Mohammadian, Simultaneous estimation of battery electric vehicle adoption with endogenous willingness to pay, ETransportation 1 (2019) 100008; (c) Y.-w. Pan, Y. Hua, S. Zhou, R. He, Y. Zhang, S. Yang, X. Liu, Y. Lian, X. Yan, B. Wu, A computational multi-node electro-thermal model for large prismatic lithium-ion batteries, J. Power Sources 459 (2020) 228070.
[3] D. Keiner, M. Ram, L.D.S.N.S. Barbosa, D. Bogdanov, C. Breyer, Cost optimal self–consumption of PV prosumers with stationary batteries, heat pumps, thermal energy storage and electric vehicles across the world up to 2050, Sol. Energy 185 (2019) 406–423.
[4] Y. Ping, H. Shen, L. Lu, C. Diao, J. Sun, Y. Gao, M. Tian, General Steps and Technical Principles of Electric Vehicle (EV) Charging Facility Planning, in: 2020 5th Asia Conference on Power and Electrical Engineering (ACPEE), IEEE, 2020, pp. 1180–1186.
[5] M. Yang, L. Zhang, W. Dong, Economic Benefit Analysis of Charging Models Based on Differential Electric Vehicle Charging Infrastructure Subsidy Policy in China, Sustain. Cities Soc. 59 (2020) 102206.
[6] J. Yu, P. Yang, K. Zhang, F. Wang, L. Miao, Evaluating the effect of policies and the development of charging infrastructure on electric vehicle diffusion in China, Sustainability 10 (10) (2018) 3394.
[7] Y. Lin, W. Ming, The development of air duct and air-cooled 60kw DC charging station based on Flotherm, Mach. Des. Manuf. Eng., 2018.
[8] W. Xiangqin, Existing bottleneck problems and countermeasures in China's electric vehicle development [J], Energy Technol. Econ. 23 (3) (2011) 1–5.
[9] T. Gan, T. Ming, W. Fang, Y. Liu, L. Miao, K. Ren, M.H. Ahmadi, Heat transfer enhancement of a microchannel heat sink with the combination of impinging jets, dimples, and side outlets, J. Therm. Anal. Calorim. (2019) 1–12.
[10] (a) S. Yang, C. Ling, Y. Fan, Y. Yang, X. Tan, H. Dong, A review of lithium-ion battery thermal management system strategies and the evaluate criteria, Int. J. Electrochem. Sci. 14 (7) (2019) 6077–6107; (b) J. Mathew, S. Krishnan, A Review on Transient Thermal Management of Electronic Devices, J. Electron. Packag. 144 (1) (2021).
[11] (a) W.T. Kim H. Nho K. In Kim Effect of heat transfer on air jet impingement of electronics componentsProceeding International Electronic Packaging Conference 1993 58-68; (b) E.C. De Jong J. Ferreira P. Bauer Design techniques for thermal management in switch mode converters. IEEE Trans. Ind. Appl. 42 (6)2006; 1375-1386; (c) S.S. Anandan V. Ramalingam. Thermal management of electronics: a review of literature Thermal Sci. 12 (2) 2008;5-26.
[12] T. Yuksel, S. Litster, V. Viswanathan, J.J. Michalek, Plug-in hybrid electric vehicle LiFePO4 battery life implications of thermal management, driving conditions, and regional climate, J. Power Sources 338 (2017) 49–64.
[13] W. Wang, H. Bian, X. Zhang, X. Fang, X. Zhou, Protective Design of DC Charger Based on Forced Air Cooling, in: 2019 11th International Conference on Intelligent Human-Machine Systems and Cybernetics (IHMSC), IEEE, 2019, pp. 308–311.
[14] W. Zhou, Y. Li, Z. Chen, L. Deng, Y. Gan, Effect of the passage area ratio of liquid to vapor on an ultra-thin flattened heat pipe, Appl. Therm. Eng. 162 (2019) 114215.
[15] R.J. McGlen, R. Jachuck, S. Lin, Integrated thermal management techniques for high power electronic devices, Appl. Therm. Eng. 24 (8-9) (2004) 1143–1156.
[16] R. Miorini, D.J. Sharar, A.V. Gowda, C. Hoel, B. Whalen, P. de Bock, A novel package-integrated cyclone cooler for the thermal management of power electronics, J. Electron. Packag. (2021).
[17] X. Yang, Y. Yan, D. Mullen, Recent developments of lightweight, high performance heat pipes, Appl. Therm. Eng. 33 (2012) 1–14.
[18] I. Mudawar, Two-Phase Microchannel Heat Sinks: Theory, Applications, and Limitations, J. Electron. Packag. 133 (4) (2011).
[19] E. Jiaqiang, D. Han, A. Qiu, H. Zhu, Y. Deng, J. Chen, X. Zhao, W. Zuo, H. Wang, J. Chen, Orthogonal experimental design of liquid-cooling structure on the cooling effect of a liquid-cooled battery thermal management system, Appl. Therm. Eng. 132 (2018) 508–520.
[20] Y. Li, W. Zhou, J. He, Y. Yan, B. Li, Z. Zeng, Thermal performance of ultra-thin flattened heat pipes with composite wick structure, Appl. Therm. Eng. 102 (2016) 487–499.
[21] H. Aoki, N. Shioya, M. Ikeda, Y. Kimura, Development of ultra thin plate-type heat pipe with less than 1 mm thickness, in: 2010 26th Annual IEEE Semiconductor Thermal Measurement and Management Symposium (SEMI-THERM), IEEE, 2010, pp. 217–222.
[22] W. Zhou, Y. Li, Z. Chen, L. Deng, Y. Gan, Ultra-thin flattened heat pipe with a novel band-shape spiral woven mesh wick for cooling smartphones, Int. J. Heat Mass Transfer 146 (2020) 118792.
[23] W. Zhou, Y. Li, Z. Chen, L. Deng, Y. Gan, A novel ultra-thin flattened heat pipe with biporous spiral woven mesh wick for cooling electronic devices, Energy Convers. Manage. 180 (2019) 769–783.
[24] M. Ivanova, A. Lai, C. Gillot, N. Sillon, C. Schaeffer, F. Lefevre, M. Lallemand, E. Fournier, Design, fabrication and test of silicon heat pipes with radial microcapillary grooves, in: Thermal and Thermomechanical Proceedings 10th Intersociety Conference on Phenomena in Electronics Systems, 2006. ITHERM 2006, IEEE, 2006, pp. 545–551.
[25] Y. Tang, S. Hong, S. Wang, D. Deng, Experimental study on thermal performances of ultra-thin flattened heat pipes, Int. J. Heat Mass Transfer 134 (2019) 884–894.
[26] B. Yan, C. Wang, L. Li, The technology of micro heat pipe cooled reactor: a review, Ann. Nucl. Energy 135 (2020) 106948.
[27] (a) W. Srimuang, P. Amatachaya, A review of the applications of heat pipe heat exchangers for heat recovery, Renewable Sustainable Energy Rev. 16 (6) (2012) 4303–4315; (b) H.N. Chaudhry, B.R. Hughes, S.A. Ghani, A review of heat pipe systems for heat recovery and renewable energy applications. *Renewable and sustainable*, Energy Rev. 16 (4) (2012) 2249–2259.
[28] H. Tang, Y. Tang, Z. Wan, J. Li, W. Yuan, L. Lu, Y. Li, K. Tang, Review of applications and developments of ultra-thin micro heat pipes for electronic cooling, Appl. Energy 223 (2018) 383–400.
[29] (a) G. Zhou, J. Li, L. Lv, An ultra-thin miniature loop heat pipe cooler for mobile electronics, Appl. Therm. Eng. 109 (2016) 514–523; (b) J. Li, L. Lv, Experimental studies on a novel thin flat heat pipe heat spreader, Appl. Therm. Eng. 93 (2016) 139–146; (c) M.S. Ahamed, Y. Saito, K. Mashiko, M. Mochizuki, Characterization of a high performance ultra-thin heat pipe cooling module for mobile hand held electronic devices, Heat Mass Transfer 53 (11) (2017) 3241–3247.
[30] C. Chen, D. Qiu, F. Hou, F. Liu, M. Su, Q. Wang, L. Cao, L. Wan, Thermal characterization of a novel 3D stacked package structure by CFD simulation, in: 2016 17th International Conference on Electronic Packaging Technology (ICEPT), IEEE, 2016, pp. 597–602.
[31] A. Ama, A. Ash, A. Tam, B. Sana, Thermal management and performance enhancement of data centers architectures using aligned/staggered in-row cooling arrangements, Case Studies in Thermal Engineering (2021).
[32] A.A. Ameri, A.In Arnone, Prediction of turbine blade passage heat transfer using a zero and a two-equation turbulence model, Turbo Expo: Power for Land, Sea, and Air, American Society of Mechanical Engineers, 1994 V004T09A015.
[33] A. Faghri, Review and advances in heat pipe science and technology, J. Heat Transfer 134 (12) (2012).
[34] H. Wang, A.K. Prasad, S.G. Advani, Hydrogen storage systems based on hydride materials with enhanced thermal conductivity, Int. J. Hydrogen Energy 37 (1) (2012) 290–298.
[35] G. Huang, W. Liu, Y. Luo, Y. Li, H. Chen, Fabrication and thermal performance of mesh-type ultra-thin vapor chambers, Appl. Therm. Eng. 162 (2019) 114263.
[36] Meyer, G. Focused on Thermal Management, TIMs, Fans, Heat Sinks, CFD Software, LEDs/Lighting.
[37] A. Bhattacharya, R.L. Mahajan, Finned Metal Foam Heat Sinks for Electronics Cooling in Forced Convection, J. Electron. Packag. 124 (3) (2002) 155–163.
[38] C. Lan, J. Xu, Y. Qiao, Y. Ma, Thermal management for high power lithium-ion battery by minichannel aluminum tubes, Appl. Therm. Eng. 101 (2016) 284–292.